Analysis of Nail Board Measurement of Liquid Slag Layer Depth

Adnan Akhtar[1], Brian G. Thomas[1, 2], Joydeep Sengupta[3]

[1]Department of Mechanical Science and Engineering
University of Illinois at Urbana-Champaign
1206 West Green Street, Urbana, IL, USA, 61801
Phone: +1-217-979-5478
Email: amakhta2@illinois.edu

[2]Department of Mechanical Engineering, Brown Hall W370-B
Colorado School of Mines
1610 Illinois Street, Golden, CO, USA, 80401
Phone: +1-303-273-3309
Email: bgthomas@mines.edu

[3]ArcelorMittal Global R&D Hamilton
1390 Burlington Street East, Hamilton, ON, Canada L8N 3J5
Phone: +1-905-548-4739
Email: joydeep.sengupta@arcelormittal.com

Keywords: Continuous casting, Nail board, Liquid slag layer measurement, Steel nail, Aluminum wire, Computational model

INTRODUCTION

The slag layer added on top of the molten steel plays an important role in the continuous casting process. It provides thermal insulation, prevents steel re-oxidation, controls the horizontal heat transfer and improves the cleanliness of the steel by entrapping inclusions. The powder added on top of the molten steel melts to form a sintered layer, eventually forming a liquid slag layer. The depth of the liquid slag layer influences the consumption of slag into the gap between the mold and the shell, its effectiveness at lubrication, and the extraction of detrimental inclusions from the molten steel into the slag [1].

The nail board test is an inexpensive technique used to measure the molten steel surface velocity and profile of the molten steel surface [2, 3]. The test is performed by inserting one or two rows of ~10 steel nails in a long wooden board. The nails and wires are dipped straight down through the top surface powder layers into the molten steel. A lump of steel is formed due to solidification of the molten steel on the cold nail surface. The nail lump positions plotted together can be used to observe the steel meniscus shape. The nails are generally dipped for 3-4 s to prevent re-melting and solidification of the lump formed. The direction of the flow on the steel top surface can be determined by observing the high end of the lump formed as it represents the instantaneous direction from which the steel flow impinges on the nail. The height difference between the high and low ends of the lump can be used to measure the surface velocity [4].

Aluminum wires are often added to the nail board test to measure the liquid slag layer depth [5, 6]. The distance from the solidified lump on the steel nail to the shortened (melted) end of the aluminum wire is measured as the molten slag layer thickness. This method assumes that the slow rate of aluminum melting in the solid powder prevents the aluminum (melting temperature ~660 °C) from melting beyond the liquid slag layer (melting temperature 900-1200 °C). Alternatively, copper wires might be employed instead of aluminum.

The objective of this study is to investigate the accuracy of the current methods used for measurement of the liquid slag layer depth. In addition, a new methodology for measuring the liquid slag layer depth is proposed, using just the steel nails themselves without a second wire. This technique is based correlating the temperature associated with the oxide colors observed during tempering on the steel nail with their location along the nail. For this investigation, a transient thermo-fluid model of the nail and wire dipping process has been developed using ANSYS Fluent. The model is validated using experimental data from steel nail dipping tests in a typical caster. The model is then run for aluminum and copper wires to

evaluate the expected difference between the measured and actual liquid slag layer thickness. The effect of process conditions and slag properties on the optimal dipping time was also investigated.

EXPERIMENTAL PROCEDURE

In the present work, 12 nail / wire dipping trials were conducted in the No. 1 continuous caster at ArcelorMittal Dofasco. Combinations of an individual steel nail, aluminum and copper wires were dipped through the slag layer into the molten steel, instead of a nail-board. The nail and wire holder, shown in Figure 1, included a flat plate that was held at the top of the powder layer during the trial. Thus, the total powder/slag thickness was measured as the distance from the lump to the plate. The nail and wire were separated by ~10mm. The casting conditions for the trials are given in Table I. The measured total powder/slag thicknesses for the trials are shown in Table II, along with the dipping times and other parameters for each test.

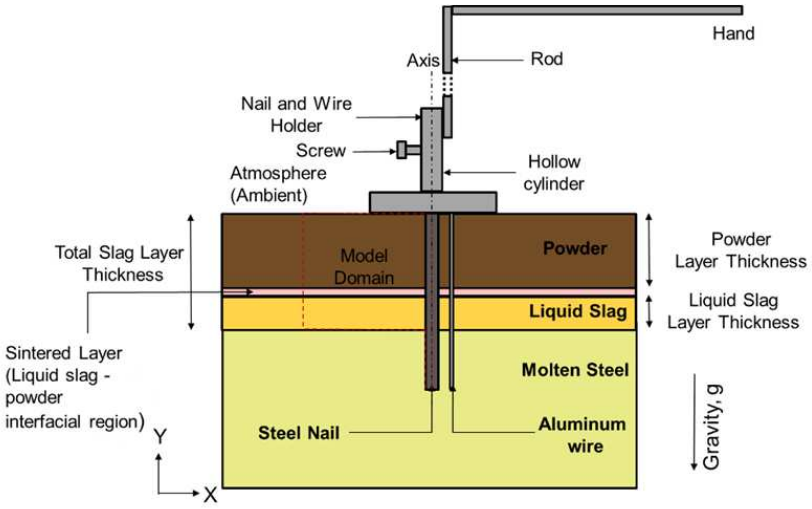

Figure 1: Schematic of the nail and wire dipping experiment in a continuous caster

Table I: Casting Conditions

Steel Grade	HSLA
Slab Width	1382 mm
Slab Thickness	220 mm
Oscillation Stroke	7 mm
Casting speed (v_s)	1 and 1.2 m/min
Oscillation frequency	93 and 111.6 cpm

Table II: Nail Dipping Trials

Trial No.	Casting Speed (m/min)	Dipping Time (s)	Oscillation Frequency (cpm)	Total Powder/Slag Thickness (mm)
101	1.2	3	111.6	64
102	1.2	4	111.6	55
103	1.2	5	111.6	56
104	1.2	3	111.6	51
105	1	3	93	59
106	1	3	93	56
107	1	3	93	63
108	1	4	93	59
109	1	4	93	58
110	1	5	93	64
111	1	5	93	53
112	1	8	93	56

The steel nail exhibits different colors, as shown in Figure 2. The locations of the color bands depend on the temperature attained during the tempering heat treatment experienced during the dipping trial. The color variation with temperature observed on the steel nail during tempering is shown in Figure 3 [7]. For temperatures above 427 °C, steel atoms radiate photons producing incandescent colors, which turn back to grey after the nail cools down. On the other hand, at temperatures below 427 °C, the heating of the steel produces an oxide layer on the surface, which has different colors according to the maximum temperature attained. These colors are visible after the steel has cooled down, and were used to determine the temperature profile along the nail during the dipping test.

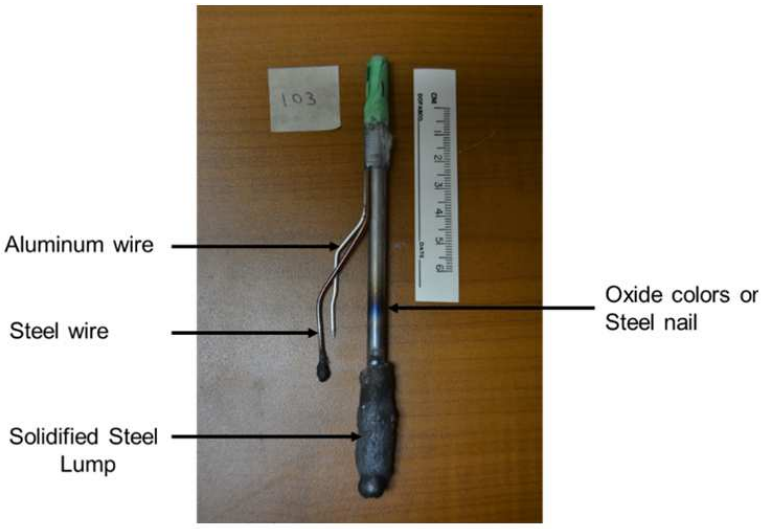

Figure 2 Photograph of steel nail along with steel and aluminum wires dipped in the continuous caster for 5 s (Trial 103)

2000°F	Bright yellow	1093°C
1900°F	Dark yellow	1038°C
1800°F	Orange yellow	982°C
1700°F	Orange	927°C
1600°F	Orange red	871°C
1500°F	Bright red	816°C
1400°F	Red	760°C
1300°F	Medium red	704°C
1200°F	Dull red	649°C
1100°F	Slight red	593°C
1000°F	Very slight red, mostly grey	538°C
0800°F	Dark grey	427°C
0575°F	Blue	302°C
0540°F	Dark Purple	282°C
0520°F	Purple	271°C
0500°F	Brown/Purple	260°C
0480°F	Brown	249°C
0465°F	Dark Straw	241°C
0445°F	Light Straw	229°C
0390°F	Faint Straw	199°C

Figure 3: Colors observed on steel during tempering at different temperatures [7]

Because particular color bands extend for different distances along the nail, the transition between colors was used for the measurements. It can be seen from the nail photograph in figure 2 that the dominant colors are grey, blue, purple and brown. Three transitions were chosen: grey to blue, blue to purple and purple to brown, which correspond to 365 °C, 292 °C and 260 °C respectively. In addition to measuring the distances of these transition lines from the lump on each nail, the surface temperature of the powder layer was measured periodically with an optical pyrometer.

COMPUTATIONAL MODEL DEVELOPMENT

Governing Equations

An axisymmetric transient thermo-fluid model has been developed to predict the temperature in the slag and nail. The model solves the energy equation given by:

$$\rho C_P \frac{\partial T}{\partial t} + \rho C_P \vec{\nabla}.(\vec{v}\, T) = \vec{\nabla}.(k_t \nabla T) \tag{1}$$

where ρ is the density, v is the velocity, k_t is the thermal conductivity and C_P is the specific heat. The slag consumption is simulated by defining a constant uniform downward axial velocity v_a throughout the simulation time.

Mesh and Boundary Conditions

Figure 4 shows the axisymmetric model domain, which contains a solid and a fluid region. The fluid region consists of the powder, sintered and the liquid slag layer which moves downward at v_a. The solid region consists of the stationary steel nail with a 3 mm radius. In the domain shown, the total powder/slag thickness is 55 mm (Trial 102). The fluid domain length was chosen to be 60 mm such that the boundary does not influence the coupled heat transfer between the nail and the slag layer. The nail length dipped in the molten steel is considered to be 30 mm based on approximate size of the lumps observed from the experiment.

A constant temperature 1550 °C (1823 K) was defined on the bottom boundary of the slag and the nail to incorporate the effect of the molten steel. From plant data for a 55 mm total powder/slag layer thickness, pyrometer measurements of the powder surface temperature were 300-325 °C. Thus, the top surface temperature of the fluid region was fixed at 312 °C (585 K). The interface between the nail and slag layers (fluid and solid regions) was defined as a coupled boundary with the slag/powder that contacts the nail equal to the temperature of the corresponding nail surface. The nail centerline is the domain axis while the boundary cutting across the top of the nail is adiabatic. The left boundary in the slag layer is also adiabatic. To simulate a domain with a wire, the only difference is to decrease the width of the solid region from 3 to 0.8 mm (wire diameter = 1.6 mm).

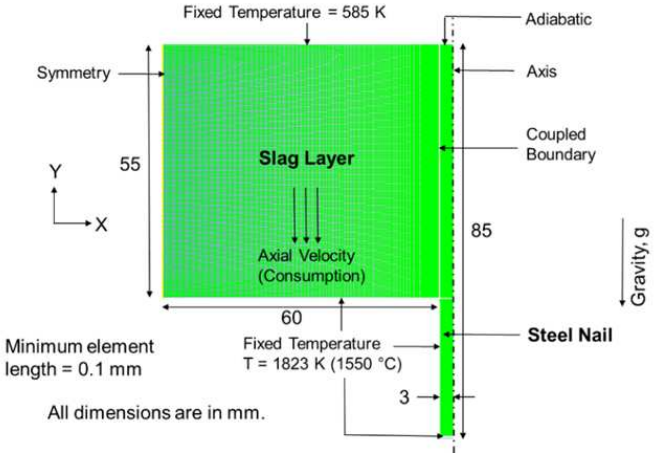

Figure 4: Schematic of model domain, mesh and boundary conditions

To find the initial condition, a simulation is performed with the coupled boundary set to zero heat flux, which gives the steady state temperature in the slag layer. Next, the temperature in the nail is initialized to ambient temperature (300 K). Then, the transient simulation described above is run with a time step size of 0.005 s with a maximum of 20 iterations per time step to achieve convergence, defined when the residual was less than 10^{-6}.

Material Properties

In the fluid region, the mold powder and slag properties vary significantly with composition and temperature. Also, the entrapment of particles from the molten steel such as alumina have a significant effect on the slag properties [8]. The solidification temperature of the slag was measured to be 1125 °C with a softening point temperature of 1020 °C. As a result,

the sintered temperature range considered for the simulation is 1027 °C – 1127 °C. A constant density of 2600 kg/m^3 is used. The thermal conductivity and specific heat are shown in Figure 5.

The thermal conductivity is defined for the melting of the powder [9]. The powder has a low thermal conductivity of 0.5 W/m K at room temperature due to the presence of air between the powder particles. With increasing temperature, the powder thermal conductivity increases due to the disappearance of the air. When the powder coalesces in the thin sinter layer, the thermal conductivity has a significant jump and reaches 2 W/m K. The liquid slag thermal conductivity increases to 3 W/m K at 1550 °C, as the effect of convection in the liquid pool and radiation become significant at higher temperatures, and locations near the molten steel.

The slag specific heat shows a significant increase at the glass transition temperature due to the enthalpy of transition between the liquid slag and solid [10]. The solid steel, copper and aluminum properties used in the simulations are shown in Table III.

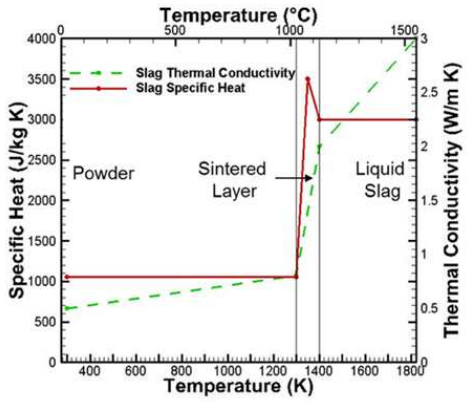

Figure 5: Temperature-dependent powder / slag thermal conductivity and specific heat

Table III: Material properties for steel, aluminum and copper [11]

Property	Steel	Aluminum	Copper	Unit
Density	7600	2719	8940	kg/m^3
Specific Heat	490	871	390	J/kg K
Thermal Conductivity	33	202.4	400	W/m K
Melting temperature	1823 (1550)	933 (660)	1358 (1085)	K (°C)

The melting of aluminum or copper wires might change the thermal properties in the melted portion of the wire (solid region) at temperatures greater than the melting temperature to be a mixture of slag and molten metal. Due to the small wire diameter, it was assumed that this molten metal was carried away by convection flow in the liquid slag layer, so slag properties should be a reasonable assumption. A schematic of the aluminum wire dipping is shown in Figure 6. Below the melting point of Aluminum (933 K), the wire is solid aluminum. Above this temperature, the melted region is filled with slag properties (next to the slag layers).

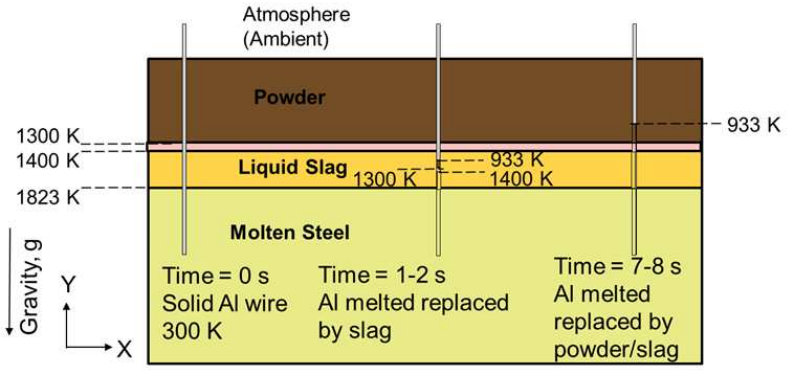

Figure 6: Schematic of the aluminum wire dipping experiment in a continuous caster with behavior in the melted region

The thermal properties assumed in the solid zone of the aluminum-melted and copper-melted wires are shown in figures 7 and 8 respectively. Density in the wire (solid region) remains that of the metal.

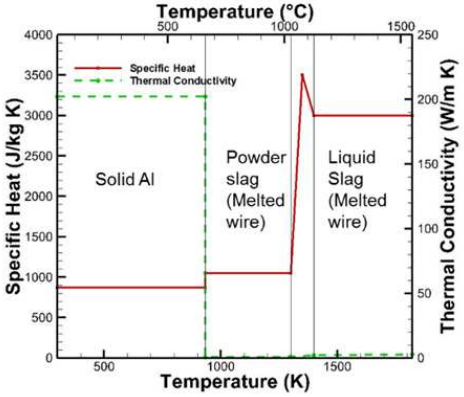

Figure 7: Temperature-dependent thermal conductivity and specific heat in the solid region for an aluminum wire

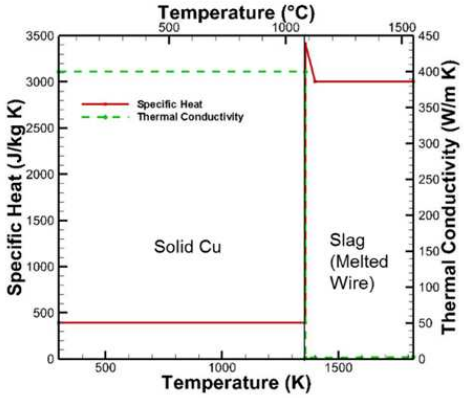

Figure 8: Temperature-dependent thermal conductivity and specific heat in the solid region for a copper wire

Flux Consumption Calculation

The flow in the powder / slag due to the slag consumption is taken into account through a downward axial velocity, v_a. The slag consumption per unit area (Q) is determined using the following relation:

$$Q\ (\frac{kg}{m^2}) = q_c\ \frac{f}{v_s} \tag{2}$$

where v_s is the casting speed, f is the oscillation frequency and q_c is the slag consumption per unit length per cycle. The latter value is calculated using an empirical relation developed by Shin *et al* [12] based on the oscillation mark consumption and lubrication consumption given by:

$$q_c = (q_{OM} + q_{lub})\ g/m\ cycle \tag{3}$$

$$q_{OM} = 2.5 \times 10^{-2} \times \rho_{slag} \times k^{1.43} \times t_n^{0.389} \times v_s^{-1.49} \times \left(\sqrt{\frac{2\,\Delta\gamma}{\Delta\rho\, g}}\right)^{0.556} \tag{4}$$

$$q_{lub} = 0.507\ e^{(3.59\ x\ t_P)} \tag{5}$$

where t_P and t_n are the positive and negative strip times respectively, v_s is the casting speed (mm/s), $\Delta\rho$ is the density difference between the liquid slag and steel (kg/m^3), $\Delta\gamma$ is the surface tension between the liquid slag and steel (N/m), g is the acceleration due to gravity and k is an empirical constant that depends on the powder properties. q_{OM} and q_{lub} are the

consumption due to the oscillation mark and lubrication respectively with units of g/m-cycle. The negative and positive strip times are calculated using the following equations [13]:

$$t_n = \frac{1}{\pi f} \cos^{-1}\left(\frac{v_s}{\pi s f}\right) \tag{6}$$

$$t_p = T - t_n \tag{7}$$

where s is the oscillation stroke and T is the total cycle time.

The downward axial velocity,v_a is calculated from the total slag consumption per second (q_{t_T}) using the slab geometry and slag density. The relations for the conversion of the total slag consumption per unit length per cycle (q_c) to total slag consumption per second and axial velocity are as follows:

$$q_s = (q_c \, x \, f) \; g/m \, s \tag{8}$$

$$q_{t\_T} = q_s \, x \, slab \; perimeter = q_s \, x \, 2(t + w) \tag{9}$$

$$v_a = \frac{q_{t\_T}}{Slab \; Area \; x \; \rho_{slag}} \tag{10}$$

For calculating the flux consumption, measurements of the consumption variation with casting speed are known as shown in Figure 9. Based on the measured values, Shin's equation [12] has been plotted as a function of the casting speed. The empirical constant *k* for the powder was chosen to be 17.8 based on the curve that best fits the measured consumption data. The parameters used for evaluating the consumption in Shin's equation are shown in Table IV.

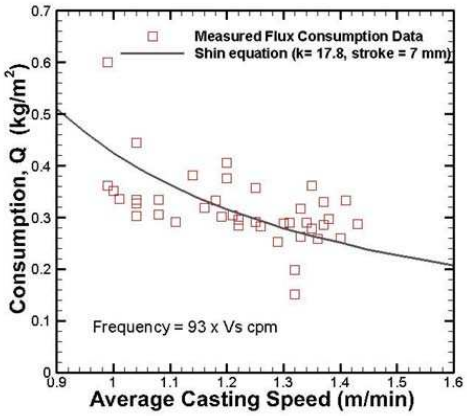

Figure 9: Comparison of measurements and Shin's equation [12] for flux consumption variation with casting speed

Table IV: Parameters used for flux consumption calculation

Density of slag	2600 kg/m^3
Density difference between slag and steel (Δρ)	4527 kg/m^3
Surface tension between the liquid slag and steel (Δγ)	1.3 N/m
Stroke (s)	7 mm
Empirical constant (k)	17.8
Slab Thickness	0.22 m
Slab Width	1.382 m

RESULTS AND DISCUSSION

Model Validation with a Steel Nail

The model is validated with measurements for two casting speeds (1 and 1.2 m/min) and three dipping times (4, 5 and 8 s). The total powder/slag layer thickness defined for these simulations is 55 mm.

Trials 102 and 103

Trial 102 was dipped for 4 s while Trial 103 was dipped for 5 s. Using Shin's correlation [12] for a 1.2 m/min casting speed, the consumption is found to be 0.315 kg/m^2. The corresponding downward axial speed found using equations 2, 8-10 is 0.0256 mm/s. The temperature contours for dipping times of 3s, 4s, and 5s are shown in Figure 10. It can be seen that the nail temperature increases with an increase in the dipping time.

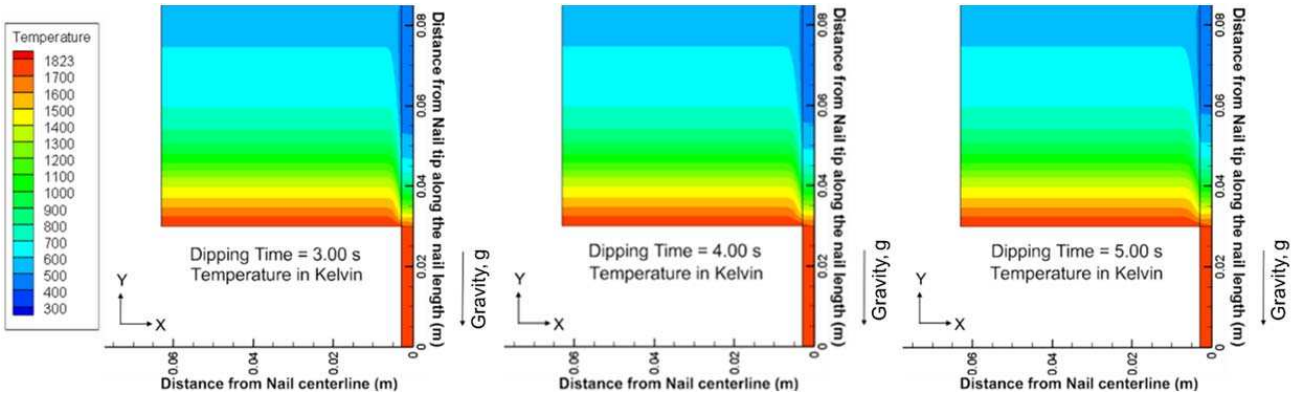

Figure 10: Temperature contours for casting speed = 1.2 m/min and dipping times 3, 4 and 5 s

A comparison of the measured distances of the 3 oxide color transitions with the predictions of those measurements, based on the simulated nail surface temperature profiles with the simulations, are shown in Figure 11 for both trials. The predictions match the measurements quite reasonably well.

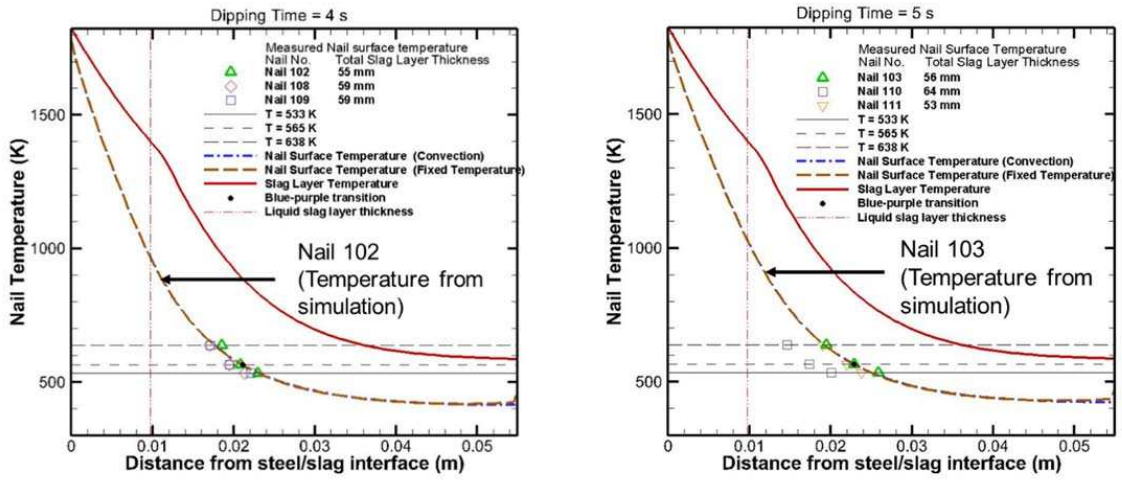

Figure 11: Simulation results with comparison of predicted and measured distances of transition temperatures for Trial 102 (left) and Trial 103 (right)

Other trials

Figure 11 also shows measurements from other nail trials, dipped for the same amount of time but having lower casting speed, (1m/min) and also different total powder/slag layer thickness. The decrease in casting speed leads to higher slag consumption (Figure 9). The accompanying higher axial velocity causes lower temperature at any given location in the slag /

powder. This is observed indirectly from the lower nail temperatures (shift of the measured color transitions to the left) in Figure 11 for Trials 108, 109, 110, and 111. The liquid slag layer thickness naturally decreases as well. In addition, it can be seen for Trial 110 that increasing the total powder/slag layer thickness may have caused the powder temperatures to decrease further.

To confirm this trend with lower casting speed, a simulation was run for Trial 112 (casting speed of 1m/min). In addition, this trial was conducted for a longer dipping time of 8 s. The total powder/slag layer thickness measured for this trial of 56 mm is close to the 55mm thickness assumed in the simulation. The slag consumption for a 1 m/min casting speed was found out to be 0.425 kg/m^2. The corresponding downward axial velocity was determined to be 0.0288 mm/s. As shown in Figure 12, the predicted locations of the nail surface temperatures match the measurements for Trial 112. The interior slag temperature is slightly lower than that of Figure 11, as expected with the lower casting speed. The nail temperatures are higher than those in Figure 11, of course, due to longer dipping time. The effect of increasing dipping time on increasing the distance along the nail of a typical temperature (i.e. the blue / purple transition temperature) is shown in Figure 13. Very short times are not shown, owing to problems with model accuracy during the act of dipping.

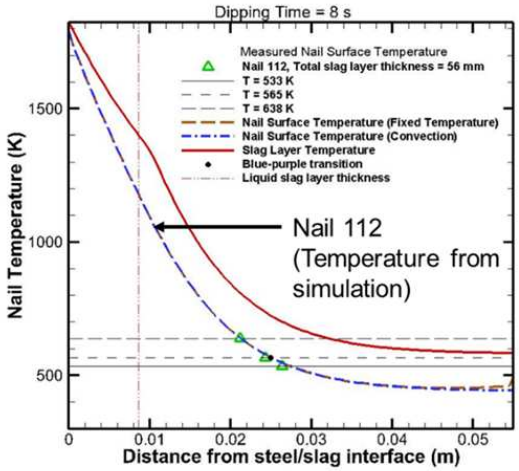

Figure 12: Comparison of predicted and measured distances of transition temperatures for Trial 112

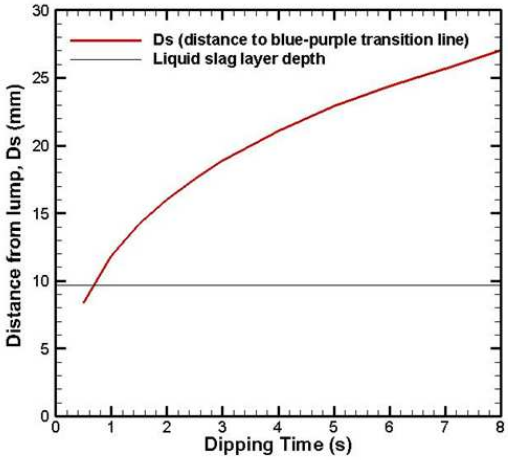

Figure 13: Simulated evolution of 565 K (292 °C) isotherm on nail surface during nail dipping test

New Method to Measure Slag Depth

The color transitions on the dipped nail can be used to measure the liquid slag layer thickness, D. Since the blue to purple color transition is most prominently visible on the steel nail, the distance from this line to the steel lump, D_S, is easy to measure in practice. It can be seen in figures 11 and 12 that this blue-purple transition line (292 °C) is much farther away from the lump (deeper) than the liquid slag layer depth. To determine the liquid slag layer thickness, the new method corrects this by multiplying this measured distance by a ratio R_S, D/Ds. This ratio is found to vary with dipping time and slag consumption, as investigated in the next sections.

$$\text{Slag layer thickness, } D = D_S \times R_S \tag{11}$$

Effect of dipping time

It can be seen from the temperature contours that with an increase in nail dipping time, the temperature along the nail surface also increases. The ratio of the liquid slag layer depth to the distance of blue-purple transition from the lump, R_S, has been calculated for different dipping times for a 55 mm total powder/slag layer thickness and a slag consumption of 6.31 g/m-s (axial velocity = 0.0256 mm/s) and is shown in Table V. The ratio decreases with an increase in the dipping time. Thus, the dipping time is an important factor in determination of the liquid slag layer depth.

Table V: Effect of nail dipping time on % liquid slag layer depth/distance from nail dipping test

Nail Dipping Time (s)	Liquid slag layer depth, D (mm)	Distance of blue-purple transition from lump, D_S (mm)	% Liquid slag layer depth/distance to blue-purple transition from lump, R_S
2s	9.7 mm	16.0 mm	60.6 %
3 s	9.7 mm	18.9 mm	51.3 %
4 s (Trial 102)	9.7 mm	21.1 mm	46.0 %
5 s (Trial 103)	9.7 mm	22.9 mm	42.4 %
8 s	9.7 mm	27.0 mm	35.9 %

Effect of slag consumption

The effect of slag consumption is studied for a total powder/slag layer thickness of 55 mm with a dipping time of 3 s. The % ratio is computed and is shown in Table VI. It can be seen that the slag consumption does not have a significant effect on the ratio. For a 3 s dipping time, a ratio of R_S=~50% of the measured distance from the lump to blue-purple transition gives the liquid slag layer depth.

Table VI: Effect of slag consumption on % liquid slag layer depth/distance from nail dipping test

Slag consumption (g/m s)	Downward axial velocity, v_a (mm/s)	Liquid slag layer depth, D (mm)	Distance of blue-purple transition from lump, D_S (mm)	% Liquid slag layer depth/distance to blue-purple transition from lump, R_S
5.83 g/m s	0.0236 mm/s	10.5 mm	21.5 mm	48.8 %
6.31 g/m s	0.0256 mm/s	9.7 mm	18.9 mm	51.3 %
7.08 g/m s	0.0288 mm/s	8.6 mm	17.3 mm	49.7 %

Because the slag consumption has little effect on RS, it is easy to calculate the liquid slag layer depth. By dipping the nail for 3 s and measuring the distance from the lump to the blue-purple transition, the liquid slag layer depth can be determined by halving the measured the distance.

Effect of slag properties

The slag properties also have a significant role in determining the liquid slag layer depth. For the same dipping time and consumption, lower slag melting temperature increases slag (and nail) temperatures and increases the liquid slag layer thickness [14]. Increasing slag thermal conductivity decreases temperature gradient across the slag layer, which increases slag (and nail) temperature and increases liquid pool depth [14].

Evaluation of Aluminum Wire Method

The dipping of a 1.6 mm diameter aluminum wire was simulated for a slag consumption of 0.315 kg/m^2 with a downward velocity, $v_a$of 0.0256 mm/s and a total powder/slag layer thickness of 55 mm (Trial 102). Powder/slag properties were used in the wire at temperatures above the melting temperature of the 933 K. Preliminary results, including a comparison of the measured aluminum wire length and wire temperature profiles calculated at different dipping times is shown in Figure 14.

With increasing time, the wire surface temperature increases and the wire length decreases as it melts. Note that the change in wire surface temperatures between 3, 4 and 5 s are quite small. This suggests that any dipping time between 3-5 s would have similar temperature and melted wire lengths. The measured slag layer depth for the 4s dipping time of this trial was 7.1mm. The simulations predict 12.5 mm, which are ~50% higher. Further work is needed to improve the model with the Al wire.

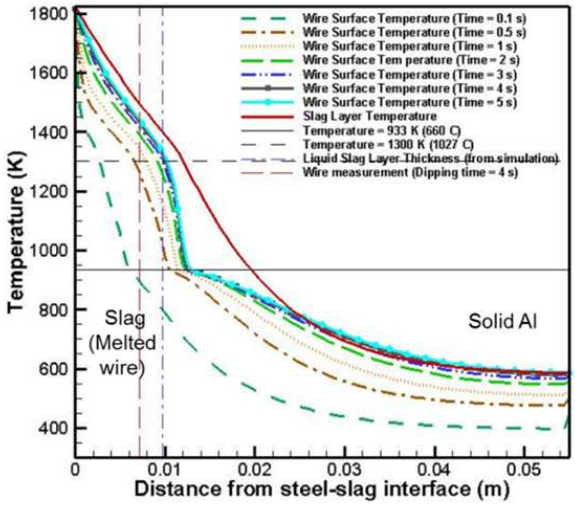

Figure 14: Aluminum wire surface temperature profiles for various dipping times

Evaluation of Copper Wire Method

A 1.6 mm diameter copper wire is also simulated for a total powder/slag layer thickness of 55 mm and a downward axial velocity, v_a of 0.0256 mm/s. The copper melts at 1358 K and the melted region contains liquid slag at temperatures above the melting temperature. The wire temperature profiles for different dipping times, and a comparison with the measured copper wire length for a different trial (Trial 105) where the powder / slag layer thickness was 59mm, are shown in Figure 14.

The copper wire predicts a liquid slag depth of 2.5 mm after a dipping time of 5 s. This is less than the measurement from the experiment of ~4mm. However, both values are very small in comparison to the liquid slag layer thickness of 9.7 mm. Due to the high thermal conductivity of the copper wire, its temperature exceeds the slag temperature in the powder after ~ 2 s but doesn't melt owing to its high melting temperature. Even if the wire is dipped longer than 15s to approach steady state, a liquid slag depth of only 4 mm is predicted. Thus, the copper wire dipping test greatly under-predicts the liquid slag layer depth.

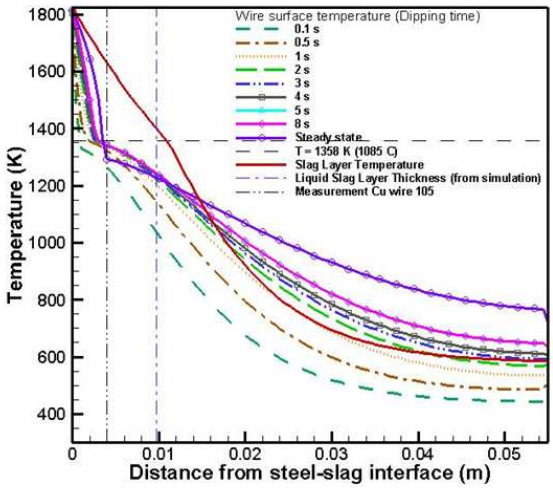

Figure 15: Copper wire surface temperature variation with dipping time and comparison with measured copper wire length (for Trial 105 with total powder/slag layer thickness 59 mm and casting speed 1 m/min)

CONCLUSIONS

This paper presents a computational model of the nail and wire dipping experiment, including slag flow due to consumption, steady temperature distribution in the powder and slag layers, and transient heat conduction in the nail and wires during the

dipping experiment. This modeling tool was validated by matching several sets of plant measurements, and applied to investigate methods to measure the liquid slag layer depth in continuous casting molds. Increasing casting speed (~20%) decreases slag consumption (~-10%), which increases slag (and nail) temperature and increases (~10%) liquid slag depth.

The main contribution of this work is to present a new method to measure the liquid slag layer depth using only a steel nail. This new method is based on the color bands of the oxide layers observed on the steel nail after dipping. For a nail dipping time of 3s, a reasonable estimate of the liquid slag layer depth is given by taking half of the measured distance from the steel lump to the blue-purple color transition line. Increasing the dipping time increases the distance, so more correction is needed (smaller R_S). The slag consumption rate has little effect.

Preliminary simulations were performed to evaluate slag layer measurement using aluminum and copper wires. The copper wire greatly under-predicts the liquid slag depth even when dipped for a long time. Further work is needed to evaluate aluminum wire dipping, and to test the new nail method in practice.

ACKNOWLEDGEMENTS

We would like to thank the member companies of the Continuous Casting Consortium at the University of Illinois, especially ArcelorMittal Dofasco for support and resources for the plant trials. We would also like to thank Jackie Leung and Bruce Farrand for help with the nail dipping trials.

REFERENCES

1. Mills, K. & Fox, A., *Metals, Slags, Glasses: High Temperature Properties & Phenomena. Mould Fluxes*, Mills Symposium, The Institute of Materials, 2002, 121-132.

2. B. Rietow and B. G. Thomas, *Using Nail Board Experiments to Quantify Surface Velocity in the CC Mold*, AISTech 2008, Pittsburgh, PA

3. R. Liu, J. Sengupta, D. Crosbie, S. Chung, M. Trinh and B.G. Thomas, *Measurement of Molten Steel Surface Velocity with SVC and Nail Dipping during Continuous Casting Process*, in Sensors, Sampling, and Simulation for Process Control, B.G. Thomas, J.A. Yurko and L. Zhang, eds., John Wiley & Sons, Hoboken, New Jersey, (TMS Annual Meeting Symposium, San Diego, CA, Feb. 27- Mar. 3, 2011), 2011, 51-58

4. R. Liu, B. G. Thomas, J. Sengupta, Stephen D. Chung and M. Trinh, *Measurements of Molten Steel Surface Velocity and Effect of Stopper-rod Movement on Transient Multiphase Fluid Flow in Continuous Casting*, ISIJ International, 2014, 54 (10), pp. 2314-2323

5. P.H. Dauby, W.H. Emling, and R. Sobolewski, *Lubrication in the Mold: A Multiple Variable System*. Ironmaker and Steelmaker, 1986. 13(Feb): p. 28-36.

6. Dauby, P.H., M.B. Assar, and G.D. Lawson, PIV and MFC Measurements in a Continuous Caster Mould. New Tools to Penetrate the Caster Black Box. La Revue de Metallurgie - CIT, 2001. 98(4): p. 353-366.

7. http://threeplanes.net/toolsteel.html, A Woodworker's Guide to Tool Steel and Heat Treating

8. E. Brandaleze, G. Di Gresia, L. Santini, A. Martín and E. Benavidez, *Mould Fluxes in the Steel Continuous Casting* Process, Science and Technology of Casting Processes, book edited by M. Srinivasan, 2012

9. McDavid, R. and B.G. Thomas, *Flow and Thermal Behavior of the Top-Surface Flux/ Powder Layers in Continuous Casting Molds*. Metall. Trans. B, 1996. 27B(4): p. 672-685

10. K.C. Mills, A. Olusanya, R. Brooks, R. Morrell and S. Bagha, Ironmaker and Steelmaker, 1988, vol. 15, pp 257-64

11. http://www.jahm.com/pages/about_mpdb.html, Material property Database (MPDB)

12. Shin, Ho-Jung, S. H. Kim, B. G. Thomas, G. G. Lee, J. M. Park, and J. Sengupta, *Measurement and Prediction of Lubrication, Powder Consumption, and Oscillation Mark Profiles in Ultra-low Carbon Steel Slabs*, ISIJ International, 2006, 46:11, 1635-1644

13. *Continuous Casting: A Practical Training Seminar*, Brian G. Thomas, AIST 2014, Indianapolis, IN

14. *Annual continuous casting consortium report*, 2015, University of Illinois Urbana-Champaign